PERGAMON

International Journal of Solids and Structures 37 (2000) 5957–5972

INTERNATIONAL JOURNAL OF SOLIDS and STRUCTURES

www.elsevier.com/locate/ijsolstr

Evaluation of stress concentration factors and stress intensity factors from remote boundary data

Chyanbin Hwu*, Y.C. Liang

Institute of Aeronautics and Astronautics, National Cheng Kung University, Tainan, Taiwan

Received 3 March 1999; in revised form 9 June 1999

Abstract

Usually, the stress concentration factors (SCFs) for holes and the stress intensity factors (SIFs) for cracks are evaluated by using the data near holes or cracks. However, the abrupt change of the stresses near holes, especially near crack tips, may lead to an unavoidable error. Thus, it is always interesting to find an equivalent formulation for SCF and SIF by using only remote boundary responses (displacements, stresses and strains) cooperating with the necessary geometric data. Through a special boundary element formulation of which the fundamental solution was derived using Stroh's formalism for two-dimensional anisotropic elasticity, all the internal stresses and strains can be expressed in terms of the boundary (not including the hole and crack boundaries) displacements and tractions. By proper mathematical manipulation, a closed form solution for SIF of the internal crack and SCF of the internal hole, expressed by using only remote boundary displacements and tractions, is derived in this paper. To show that the proposed formula is accurate and efficient, several numerical examples are presented.

Keywords: Stress concentration factor; Stress intensity factor; Hole; Crack; Boundary element; Stroh formalism; Anisotropic elasticity

1. Introduction

It is well known that the largest stress around the hole of an anisotropic body may be several times of the remote stresses, while for a cracked body, the stresses near the crack tip even exhibit a square root singularity. To denote the highest stress concentration caused by a hole or a crack, parameters like the stress concentration factor (SCF) of the hole and the stress intensity factor (SIF) of the crack are usually used. Although several analytical solutions for SCF and SIF can be found in the literature

* Corresponding author. Fax: +886-6-238-9940.
E-mail address: CHwu@mail.ncku.edu.tw (C. Hwu).

0020-7683/00/$ - see front matter
PII: S0020-7683(99)00245-0

(Savin, 1961; Murakami, 1987), they are limited to a few idealized unbounded bodies. For practical problems involving finite geometry and complex loading, numerical methods are usually employed, for which the stresses near holes or cracks are generally required (Owen and Fawkes, 1983; Anderson, 1991).

Due to singularity characteristics, more efforts have been devoted to cracked-bodies than to hole-bodies. The most famous one is the path independent J-integral proposed by Rice (1968), which can be used to calculate SIFs using data that are far removed from the crack tip. However, the J-integral cannot be applied to problems where mixed-mode SIFs are present since the value of the integral gives only the sum of SIFs. To overcome this situation, an alternative path-independent integral considering the interaction energy between the elastic state of interest and an auxiliary state was proposed by Chen and Shield (1977), and was used by Yau et al. (1980) for isotropic materials and by Wu (1989) for anisotropic materials. In this method, the stress, displacement and SIF of an auxiliary state in the same cracked body are required a priori to calculate SIF of the state of interest, which is inconvenient for complicated finite bodies.

Recently, my co-workers and I developed a special boundary element method dealing with the problems of multi-holes, cracks and inclusions (Hwu and Yen, 1991; Hwu and Liao, 1994). The special feature of this element is that no meshes are needed around the hole (or crack or inclusion) boundary. Through this boundary element, all the internal stresses and strains can be expressed in terms of displacements and tractions on the boundaries excluding the hole, crack and inclusion boundaries. Hence, even the SCF or SIF is defined by the stresses around the hole or near the crack tip and it may be calculated using the displacements and tractions on the remote boundaries. However, no explicit closed-form solution for SCF and SIF by using only the remote boundary data was found at that stage. Moreover, the shape of the hole (or inclusion) was restricted to be elliptic. In this paper, by Stroh's formalism (Stroh, 1958; Ting, 1996) and proper boundary element formulation (Hwu, 1999), explicit closed form solutions for SIF of internal straight cracks and SCF of internal elliptical or polygon-like holes are derived and expressed in terms of the remote boundary displacements and tractions. Since Stroh's formalism is for two-dimensional linear anisotropic elasticity, our results can be applied to any kind of linear anisotropic materials but is restricted to the two-dimensional problems which include generalized plane stress, generalized plane strain and anti-plane problems. To show that the proposed formula is accurate and efficient, several numerical examples are presented.

2. Green's function

2.1. Anisotropic elasticity

For a two-dimensional anisotropic linear elastic medium, the basic equations of strain–displacement, stress–strain and equilibrium may be written as

$$\epsilon_{ij} = \frac{1}{2}(u_{i,j} + u_{j,i}), \qquad \sigma_{ij} = C_{ijks}\epsilon_{ks}, \qquad \sigma_{ij,j} = 0, \tag{1}$$

where, u_i, σ_{ij} and ϵ_{ij} are, respectively, the displacement, stress and strain. The repeated indices imply summation; a comma stands for differentiation and C_{ijks} are the elastic constants which are assumed to be fully symmetric and positive definite. A general solution satisfying Eq. (1) has been presented as (Stroh, 1958; Ting, 1996)

$$\mathbf{u} = \mathbf{A}\mathbf{f}(z) + \overline{\mathbf{A}\mathbf{f}(z)}, \qquad \boldsymbol{\phi} = \mathbf{B}\mathbf{f}(z) + \overline{\mathbf{B}\mathbf{f}(z)}, \tag{2a}$$

where

$$\mathbf{A} = \begin{bmatrix} \mathbf{a}_1 & \mathbf{a}_2 & \mathbf{a}_3 \end{bmatrix}, \qquad \mathbf{B} = \begin{bmatrix} \mathbf{b}_1 & \mathbf{b}_2 & \mathbf{b}_3 \end{bmatrix},$$

$$\mathbf{f}(z) = \left[f_1(z_1), f_2(z_2), f_3(z_3)\right]^{\mathrm{T}}, \qquad z_\alpha = x_1 + p_\alpha x_2, \quad \alpha = 1, 2, 3. \tag{2b}$$

$\mathbf{u}$ and $\boldsymbol{\phi}$, are 3×1 column vectors denoting the displacements (u_1, u_2, u_3) and stress functions (ϕ_1, ϕ_2, ϕ_3). The stress function ϕ_i is related to the stresses by

$$\sigma_{i1} = -\phi_{i,2}, \qquad \sigma_{i2} = \phi_{i,1}. \tag{2c}$$

The superscript T denotes the transpose and the overline represents the conjugate of a complex number. The material eigenvalues p_α, and eigenvectors $\mathbf{a}_\alpha$, $\mathbf{b}_\alpha$ are determined by the following eigenrelations:

$$\mathbf{N}\boldsymbol{\xi} = p\boldsymbol{\xi}, \tag{3a}$$

where

$$\mathbf{N} = \begin{bmatrix} \mathbf{N}_1 & \mathbf{N}_2 \\ \mathbf{N}_3 & \mathbf{N}_1^{\mathrm{T}} \end{bmatrix}, \qquad \boldsymbol{\xi} = \begin{bmatrix} \mathbf{a} \\ \mathbf{b} \end{bmatrix}$$

$$\mathbf{N}_1 = -\mathbf{T}^{-1}\mathbf{R}^{\mathrm{T}}, \quad \mathbf{N}_2 = \mathbf{T}^{-1} = \mathbf{N}_2^{\mathrm{T}},$$

$$\mathbf{N}_3 = \mathbf{R}\mathbf{T}^{-1}\mathbf{R}^{\mathrm{T}} - \mathbf{Q} = \mathbf{N}_3^{\mathrm{T}} \tag{3b}$$

and

$$Q_{ik} = C_{i1k1}, \qquad R_{ik} = C_{i1k2}, \qquad T_{ik} = C_{i2k2}. \tag{3c}$$

$f_\alpha(z_\alpha)$, $\alpha = 1, 2, 3$, are three holomorphic functions of complex variables z_α, which will be determined by the boundary conditions set for each particular problem. The surface traction vector $\mathbf{t}$ can be calculated by using Cauchy's formula (Sokolnikoff, 1956), i.e., $t_i = \sigma_{ij}m_j$ where m_j is the unit normal to the surface boundary. If s is the arc length measured along a curved boundary, using Cauchy's formula and the relation given in Eq. (2c), we may obtain a useful formula:

$$\mathbf{t} = \frac{\partial \boldsymbol{\phi}}{\partial s} \tag{4}$$

Usually, the stress components along any other coordinate axes are calculated using the transformation law of second order tensors. Based upon the formula obtained in Eq. (4), an alternative approach to determining stress components of the rotated coordinate axes has been introduced (Ting, 1996). Let ($\mathbf{n}$, $\mathbf{m}$) be the unit vector tangent and normal to a surface boundary. By Eq. (4) we have

$$\sigma_{mm} = \mathbf{m}^{\mathrm{T}}(\theta)\boldsymbol{\phi}_{,n}, \qquad \sigma_{mn} = \mathbf{n}^{\mathrm{T}}(\theta)\boldsymbol{\phi}_{,n}, \qquad \sigma_{m3} = \left(\boldsymbol{\phi}_{,n}\right)_3,$$

$$\sigma_{nn} = -\mathbf{n}^{\mathrm{T}}(\theta)\boldsymbol{\phi}_{,m}, \qquad \sigma_{nm} = -\mathbf{m}^{\mathrm{T}}(\theta)\boldsymbol{\phi}_{,m} = \sigma_{mn}, \qquad \sigma_{n3} = -\left(\boldsymbol{\phi}_{,m}\right)_3, \tag{5a}$$

where

$$\mathbf{n}^{\mathrm{T}}(\theta) = (\cos\theta, \sin\theta, 0), \qquad \mathbf{m}^{\mathrm{T}}(\theta) = (-\sin\theta, \cos\theta, 0), \tag{5b}$$

and the angle θ is directed counterclockwise from the positive x_1-axis to the direction of $\mathbf{n}$.

2.2. Green's function for elliptical holes

Consider an infinite anisotropic plate containing a traction-free hole subjected to a point force $\hat{\mathbf{p}}$ applied at point $\hat{\mathbf{x}}$. The elasticity solution of this problem is known as Green's function for hole problems, which can also be used as a special fundamental solution for boundary element formulation. If the hole boundary shape is an ellipse or has degenerated to a crack, the associated analytical solution has been obtained as (Hwu and Yen, 1991; Wang and Tarn, 1993)

$$\mathbf{f}(z) = (\mathbf{F}_0 + \mathbf{F}_1)\hat{\mathbf{p}},$$

where

$$\mathbf{F}_0 = \frac{1}{2\pi i} \ll \log\left(\zeta_\alpha - \hat{\zeta}_\alpha\right) \gg \mathbf{A}^{\mathrm{T}},$$

$$\mathbf{F}_1 = \frac{1}{2\pi i}\sum_{k=1}^{3} \ll \log\left(\zeta_\alpha^{-1} - \bar{\hat{\zeta}}_k\right) \gg \mathbf{B}^{-1}\bar{\mathbf{B}}\mathbf{I}_k\bar{\mathbf{A}}^{\mathrm{T}} \tag{6}$$

$\ll \gg$ means a diagonal matrix in which each component is varied according to the subscript α. $\mathbf{I}_k = \ll I_\alpha^k \gg$, where $I_\alpha^1 = 1, 0, 0$, $I_\alpha^2 = 0, 1, 0$, $I_\alpha^3 = 0, 0, 1$, $\alpha = 1, 2, 3$.

$$\zeta_\alpha = \frac{z_\alpha + \sqrt{z_\alpha^2 - (a^2 + b^2 p_\alpha^2)}}{a - ibp_\alpha}, \qquad \hat{\zeta}_\alpha = \frac{\hat{z}_\alpha + \sqrt{\hat{z}_\alpha^2 - (a^2 + b^2 p_\alpha^2)}}{a - ibp_\alpha}, \tag{7}$$

and a, b are the lengths of semi-axes of the ellipse. For a straight crack, $b = 0$.

2.3. Green's function for polygon-like holes

If the hole boundary shape is not an ellipse, the solution shown in Eq. (6) may still be used except the transformation function provided in Eq. (7) should be changed. Consider a special hole, the contour of which is given by the equations (Savin, 1961; Lekhnitskii, 1968):

$$x_1 = a(\cos\varphi + \varepsilon\cos k\varphi),$$

$$x_2 = a(c\sin\varphi - \varepsilon\sin k\varphi), \tag{8}$$

where $0 < c \leq 1$, and k is an integer. Note that $\varepsilon = 0$ is the special case of an elliptical hole with semi-axes a and ac, as discussed previously. When $\varepsilon = 0$, $c = 1$ and $\varepsilon = 0$, $c \to 0$, the contour is respectively a circular hole and a crack. In the case of $c = 1$ and $k = 2$ with an appropriate selection of the parameter ε, the hole will differ little from an equilateral triangle with rounded corners (see Fig. 1). Not any composition of a, c, ε, k can have reasonable contours. Some contours with various compositions of a, c, εk, are plotted in Fig. 1, from which we see that Eq. (8) generally represents a polygon-like shape. To bring about a reduction of the rounding-off radius at the corners and a smaller deviation of the contour curves from the straight line, i.e., to have a more accurate parametric representation of a polygonal hole, an increased number of cos and sin terms are needed in Eq. (8) (Savin, 1961).

To find a substitute for Eq. (7), an infinite z-plane with a hole represented by Eq. (8) is now transformed to the infinite ζ_α-plane with a unit circle. By using Eq. (8) and the relations $z_\alpha = x_1 + p_\alpha x_2$ and $\zeta_\alpha = e^{i\varphi}$ around the unit circle, the transformation function between z_α and ζ_α is found to be (Hwu, 1990)

$$z_\alpha = \frac{a}{2}\left\{(1 - ip_\alpha c)\zeta_\alpha + (1 + ip_\alpha c)\frac{1}{\zeta_\alpha} + \varepsilon(1 + ip_\alpha)\zeta_\alpha^k + \varepsilon(1 - ip_\alpha)\frac{1}{\zeta_\alpha^k}\right\}, \quad (\alpha \text{ is not summed}), \tag{9}$$

If $\varepsilon = 0$ (elliptical hole) or $p_\alpha = i$ (isotropic materials), the transformation is one-to-one. Otherwise, the transformation function is generally not one-to-one. If we designate the point outside of but nearest to the unit circle to be the mapped point, a one-to-one transformation with cuts passing through the critical points may be obtained. With this designation for nonsingle-valued transformation, the solutions obtained will be well approximated if the critical points are far away from the hole (Hwu, 1992; Wang and Tarn, 1993). Due to the complexity of Eq. (9), it is difficult to obtain an explicit inverse function for the polygonal hole like that for the elliptical hole as shown in Eq. (7). Thus, the numerical calculation from z_α to ζ_α is necessary for the case of the general polygon-like hole.

3. Boundary element formulation

Due to the mathematical infeasibility of the finite domain problems, most of the analytical closed form solutions are obtained for the infinite domain problems. These closed form solutions are important for engineers to observe the special feature of the discussed problem, such as SIF for crack problems and SCF for hole problems. Moreover, with the aid of the analytical solutions for the infinite domain problems, most of the numerical techniques such as the finite element method and boundary element method can be improved in their accuracy and efficiency.

It is well known that Green's function plays an important role in the boundary element method. If

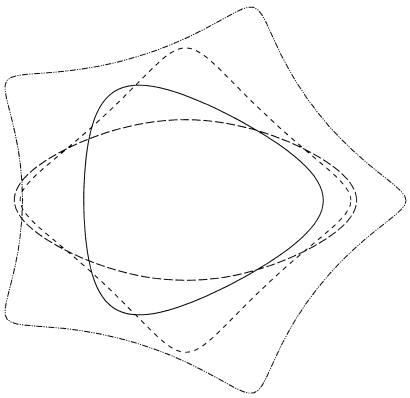

	a	c	ε	k
——	0.05	1.0	0.15	2
- - - - -	0.06	1.0	0.15	3
- - - -	0.07	0.5	0.02	3
-·-·-	0.08	1.0	0.15	4

Fig. 1. Various contours of polygon-like holes.

Green's function for the traction-free hole (or crack) problem is employed in boundary element formulation as its fundamental solution, discretization around the hole (or crack) boundary is avoided. This results in a saving of computer time and storage. Moreover, due to complete satisfaction of the hole boundary condition, discretization with relatively coarse meshes can achieve high accuracy. Based upon this concept, a linear boundary element formulation has been given in (Hwu, 1999). For the convenience of later derivation, we present here the boundary integral equation of the discretized form in which the boundary is discretized into M segments with N nodes, as shown in Fig. 2,

$$\mathbf{c}(\hat{\mathbf{x}})\mathbf{u}(\hat{\mathbf{x}}) + \sum_{m=1}^{M}\left\{\hat{\mathbf{Y}}_m^{(1)}(\hat{\mathbf{x}})\mathbf{u}_m^{(1)} + \hat{\mathbf{Y}}_m^{(2)}(\hat{\mathbf{x}})\mathbf{u}_m^{(2)}\right\} = \sum_{m=1}^{M}\left\{\mathbf{G}_m^{(1)}(\hat{\mathbf{x}})\mathbf{t}_m^{(1)} + \mathbf{G}_m^{(2)}(\hat{\mathbf{x}})\mathbf{t}_m^{(2)}\right\}, \tag{10a}$$

where

$$\hat{\mathbf{Y}}_m^{(i)}(\hat{\mathbf{x}}) = \int_{\Gamma_m} \hat{\mathbf{T}}(\hat{\mathbf{x}}, \mathbf{x})\varpi_i(\xi)\,\mathrm{d}\Gamma_m,$$

$$\mathbf{G}_m^{(i)}(\hat{\mathbf{x}}) = \int_{\Gamma_m} \hat{\mathbf{U}}(\hat{\mathbf{x}}, \mathbf{x})\varpi_i(\xi)\,\mathrm{d}\Gamma_m, \quad i = 1, 2, \tag{10b}$$

$$\mathbf{x} = \varpi_1\mathbf{x}_m^{(1)} + \varpi_2\mathbf{x}_m^{(2)},$$

$$\varpi_1 = \frac{1}{2}(1-\xi), \qquad \varpi_2 = \frac{1}{2}(1+\xi)$$

and $\hat{U}_{ij}$ and $\hat{T}_{ij}$ are, respectively, the displacements and tractions in the j-direction at point $\mathbf{x}$

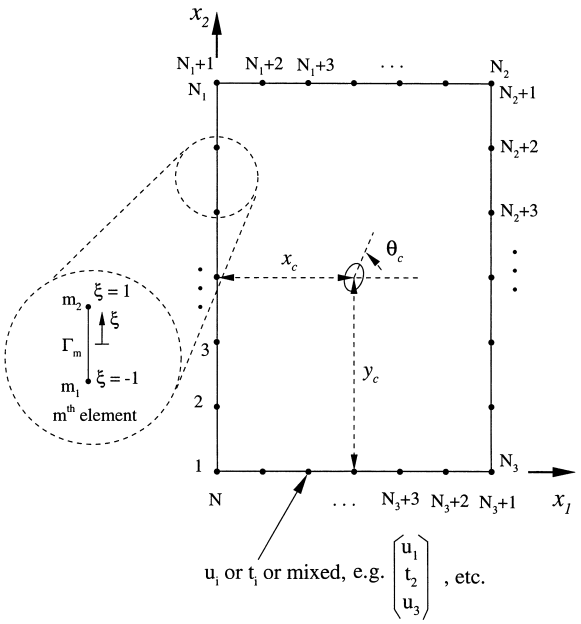

Fig. 2. Meshes, shape function and the prescribed boundary conditions.

corresponding to a unit point force acting in the i-direction applied at point $\hat{\mathbf{x}}$. The explicit formulae of $\hat{\mathbf{U}}$ and $\hat{\mathbf{T}}$ can then be obtained by substituting Eq. (6) into Eq. (2). The results are

$$\hat{\mathbf{U}} = 2\mathrm{Re}\{\mathbf{A}(\mathbf{F}_0 + \mathbf{F}_1)\}, \qquad \hat{\mathbf{T}} = 2\mathrm{Re}\{\mathbf{B}(\mathbf{F}_{0,s} + \mathbf{F}_{1,s})\} \tag{10c}$$

where

$$\mathbf{F}_{0,s} = \frac{1}{2\pi i} \ll \frac{1}{\zeta_\alpha - \hat{\zeta}_\alpha} \frac{\mathrm{d}\zeta_\alpha}{\mathrm{d}z_\alpha} \frac{\partial z_\alpha}{\partial s} \gg \mathbf{A}^{\mathrm{T}} \tag{10d}$$

$$\mathbf{F}_{1,s} = \frac{1}{2\pi i} \sum_{k=1}^{3} \ll \frac{-\zeta_\alpha^{-2}}{\zeta_\alpha^{-1} - \bar{\hat{\zeta}}_k} \frac{\mathrm{d}\zeta_\alpha}{\mathrm{d}z_\alpha} \frac{\partial z_\alpha}{\partial s} \gg \mathbf{B}^{-1}\bar{\mathbf{B}} I_k \bar{\mathbf{A}}^{\mathrm{T}}$$

and

$$\frac{\partial z_\alpha}{\partial s} = s_1 + p_\alpha s_2, \qquad s_1 = \frac{\partial x_1}{\partial s}, \quad s_2 = \frac{\partial x_2}{\partial s}$$

$$\frac{\mathrm{d}\zeta_\alpha}{\mathrm{d}z_\alpha} = \frac{2}{a}\left\{(1 - ip_\alpha c) - (1 + ip_\alpha c)\zeta_\alpha^{-2} + \varepsilon\kappa(1 + ip_\alpha)\zeta_\alpha^{\kappa-1} - \varepsilon\kappa(1 - ip_\alpha)\zeta_\alpha^{-(\kappa+1)}\right\}^{-1}. \tag{10e}$$

In Eqs. (10a) and (10b), a symbol with subscript m and superscript (1) or (2) denotes the value of node 1 or 2 of the mth element. $\hat{\mathbf{Y}}_m^{(i)}(\hat{\mathbf{x}})$ and $\mathbf{G}_m^{(i)}(\hat{\mathbf{x}})$, $i = 1, 2$ are the matrices of influence coefficients defining the interaction between the point $\hat{\mathbf{x}}$ and the particular node (1 and 2) on element m. $\mathbf{c}(\hat{\mathbf{x}})$ is a coefficient matrix dependent on the location $\hat{\mathbf{x}}$. For a smooth boundary, $\mathbf{c} = \frac{1}{2}\mathbf{I}$, where $\mathbf{I}$ is an identity matrix. For an internal point $\mathbf{c} = \mathbf{I}$. For practical applications, $\mathbf{c}$ can be computed by assuming a unit rigid body movement in any direction. The mapping function of $\zeta_\alpha(z_\alpha)$ has been given in Eq. (9) for general polygon-like holes including elliptical holes and cracks. For elliptical holes, $\varepsilon = 0$ in Eq. (9). While for cracks, $\varepsilon = 0$ and $c = 0$. The expression given in Eq. (7) is the inversion of the mapping function (9) with $\varepsilon = 0$.

Γ_m is the mth segment of the discretized boundary. To evaluate the integrals of Eq. (10b) along Γ_m, $\hat{\mathbf{T}}$ and $\hat{\mathbf{U}}$ are expressed in terms of the nondimensionless coordinate ξ, and the differential $\mathrm{d}\Gamma_m$ is transformed to $\mathrm{d}\xi$ multiplied by Jacobian $|J_m|$ as

$$\mathrm{d}\Gamma_m(\mathbf{x}) = |J_m|\mathrm{d}\xi, \qquad |J_m| = \sqrt{\left(\frac{\mathrm{d}x_1}{\mathrm{d}}\xi\right)^2 + \left(\frac{\mathrm{d}x_2}{\mathrm{d}\xi}\right)^2} = \frac{\ell_m}{2} \tag{11}$$

where ℓ_m is the length of the mth element. Substituting Eq. (11) into Eq. (10b), $\hat{\mathbf{Y}}_m^{(i)}$ and $\mathbf{G}_m^{(i)}$ can be obtained by employing a numerical integration. Since the second node of the $(m-1)$th element is the first node of the mth element, and may be named as the nth node of the entire boundary element, the components $\mathbf{Y}_m^{(i)}$ or $\mathbf{G}_m^{(i)}$ at the same node n for the neighbor elements are summed together to become $\hat{\mathbf{Y}}_n$ or $\mathbf{G}_n$. Eq. (10a) can then be rewritten as

$$\mathbf{c}(\hat{\mathbf{x}})\mathbf{u}(\hat{\mathbf{x}}) + \sum_{n=1}^{N} \hat{\mathbf{Y}}_n(\hat{\mathbf{x}})\mathbf{u}_n = \sum_{n=1}^{N} \mathbf{G}_n(\hat{\mathbf{x}})\mathbf{t}_n \tag{12}$$

Consider $\hat{\mathbf{x}}$ to be node i and use $\mathbf{c}_i$, $\mathbf{u}_i$, $\hat{\mathbf{Y}}_{in}$, $\mathbf{G}_{in}$ to denote the values of $\mathbf{c}$, $\mathbf{u}$, $\hat{\mathbf{Y}}_n$, $\mathbf{G}_n$ at node i. Define the new matrices $\mathbf{Y}_{in} = \hat{\mathbf{Y}}_{in}$, $i \neq n$; $\mathbf{Y}_{in} = \hat{\mathbf{Y}}_{in} + \mathbf{c}_i$, $i = n$. When all the nodes are taken into consideration,

Eq. (12) can finally produce a $3N \times 3N$ system of equations which can be represented in matrix form as

$$\begin{bmatrix} \mathbf{Y}_{11} & \mathbf{Y}_{12} & \dots & \mathbf{Y}_{1N} \\ \mathbf{Y}_{21} & \mathbf{Y}_{22} & \dots & \mathbf{Y}_{2N} \\ . & . & \dots & . \\ . & . & \dots & . \\ \mathbf{Y}_{i1} & \mathbf{Y}_{i2} & \dots & \mathbf{Y}_{iN} \\ . & . & \dots & . \\ . & . & \dots & . \\ \mathbf{Y}_{N1} & \mathbf{Y}_{N2} & \dots & \mathbf{Y}_{NN} \end{bmatrix} \begin{Bmatrix} \mathbf{u}_1 \\ \mathbf{u}_2 \\ . \\ . \\ \mathbf{u}_i \\ . \\ . \\ \mathbf{u}_N \end{Bmatrix} = \begin{bmatrix} \mathbf{G}_{11} & \mathbf{G}_{12} & \dots & \mathbf{G}_{1N} \\ \mathbf{G}_{21} & \mathbf{G}_{22} & \dots & \mathbf{G}_{2N} \\ . & . & \dots & . \\ . & . & \dots & . \\ \mathbf{G}_{i1} & \mathbf{G}_{i2} & \dots & \mathbf{G}_{iN} \\ . & . & \dots & . \\ . & . & \dots & . \\ \mathbf{G}_{N1} & \mathbf{G}_{N2} & \dots & \mathbf{G}_{NN} \end{bmatrix} \begin{Bmatrix} \mathbf{t}_1 \\ \mathbf{t}_2 \\ . \\ . \\ \mathbf{t}_i \\ . \\ . \\ \mathbf{t}_N \end{Bmatrix} \tag{13}$$

To solve the simultaneously linear algebraic equations shown in Eq. (13), we first input the information from the boundary conditions. That is, one of the two variables (u_i or t_i) should be known in each node. For displacement-prescribed boundary value problems, all $\mathbf{u}_i$ are known along the boundary and $\mathbf{t}_i$ will then be determined from Eq. (13). Similarly, for traction-prescribed boundary value problems, all $\mathbf{t}_i$ are known along the boundary and $\mathbf{u}_i$ are determined from Eq. (13). For mixed-boundary value problems, parts of u_i and t_i are given; all the others are determined from Eq. (13).

4. Displacements, strains and stresses of interior points

Once all the values of $\mathbf{u}_i$ and $\mathbf{t}_i$ on the boundary are determined, the values of stresses, strains and displacements at any interior point can be calculated by using Eq. (12). If $\hat{\mathbf{x}}$ is an interior point, $\mathbf{c}(\hat{\mathbf{x}}) = \mathbf{I}$. The displacement at any interior point inside the body can therefore be obtained from Eq. (12) as

$$\mathbf{u}(\hat{\mathbf{x}}) = \sum_{n=1}^{N} \left\{ \mathbf{G}_n(\hat{\mathbf{x}})\mathbf{t}_n - \hat{\mathbf{Y}}_n(\hat{\mathbf{x}})\mathbf{u}_n \right\} \tag{14}$$

By differentiating Eq. (14) with respect to $\hat{\mathbf{x}}$, and using two-dimensional strain displacement relations $\epsilon_{11} = u_{1,1}$, $\epsilon_{22} = u_{2,2}$, $\epsilon_{33} = 0$, $\epsilon_{12} = \epsilon_{21} = \frac{1}{2}(u_{1,2} + u_{2,1})$, $\epsilon_{13} = \epsilon_{31} = \frac{1}{2}u_{3,1}$, $\epsilon_{23} = \epsilon_{32} = \frac{1}{2}u_{3,2}$, the strains can directly be obtained if we know $\mathbf{u}_{,1}$ and $\mathbf{u}_{,2}$. By differentiating Eq. (14) with respect to $\hat{x}_1$ and $\hat{x}_2$, we find

$$\mathbf{u}_{,i}(\hat{\mathbf{x}}) = \sum_{n=1}^{N} \left\{ \mathbf{G}_{n,i}(\hat{\mathbf{x}})\mathbf{t}_n - \hat{\mathbf{Y}}_{n,i}(\hat{\mathbf{x}})\mathbf{u}_n \right\}, \quad i = 1, 2 \tag{15}$$

Note that $\mathbf{G}_{n,i}$ and $\hat{\mathbf{Y}}_{n,i}$ can be obtained from Eq. (10b) analytically by directly differentiating $\hat{\mathbf{T}}$ and $\hat{\mathbf{U}}$ with respect to $\hat{\mathbf{x}}$. The explicit expressions of $\hat{\mathbf{T}}_{,i}$ and $\hat{\mathbf{U}}_{,i}$ for general polygon-like holes including the elliptical holes ($\varepsilon = 0$) and cracks ($\varepsilon = 0$, $c = 0$)are:

$$\hat{\mathbf{U}}_{,i} = 2\mathrm{Re}\left\{ \mathbf{A}\left(\mathbf{F}_{0,\hat{x}_i} + \mathbf{F}_{1,\hat{x}_i} \right) \right\},$$

$$\hat{\mathbf{T}}_{,i} = 2\mathrm{Re}\left\{ \mathbf{B}\left(\mathbf{F}_{0,s\hat{x}_i} + \mathbf{F}_{1,s\hat{x}_i} \right) \right\} \tag{16a}$$

where

$$\mathbf{F}_{0,\hat{x}_i} = \frac{1}{2\pi i} \ll \frac{-1}{\zeta_\alpha - \hat{\zeta}_\alpha} \frac{\mathrm{d}\hat{\zeta}_\alpha}{\mathrm{d}\hat{z}_\alpha} \frac{\partial \hat{z}_\alpha}{\partial \hat{x}_i} \gg \mathbf{A}^{\mathrm{T}}$$

$$\mathbf{F}_{1,\,\hat{x}_i} = \frac{1}{2\pi i}\sum_{k=1}^{3} \ll \frac{-1}{\zeta_\alpha^{-1} - \bar{\hat{\zeta}}_k}\frac{\mathrm{d}\bar{\hat{\zeta}}_k}{\mathrm{d}\bar{\hat{z}}_k}\frac{\partial \bar{\hat{z}}_k}{\partial \hat{x}_i} \gg \mathbf{B}^{-1}\bar{\mathbf{B}}\mathbf{I}_k\bar{\mathbf{A}}^{\mathrm{T}} \tag{16b}$$

$$\mathbf{F}_{0,\,s\hat{x}_i} = \frac{1}{2\pi i} \ll \frac{1}{\left(\zeta_\alpha - \hat{\zeta}_\alpha\right)^2}\frac{\mathrm{d}\zeta_\alpha}{\mathrm{d}z_\alpha}\frac{\partial z_\alpha}{\partial s}\frac{\mathrm{d}\hat{\zeta}_\alpha}{\mathrm{d}\hat{z}_\alpha}\frac{\partial \hat{z}_\alpha}{\partial \hat{x}_i} \gg \mathbf{A}^{\mathrm{T}}$$

$$\mathbf{F}_{1,\,s\hat{x}_i} = \frac{1}{2\pi i}\sum_{k=1}^{3} \ll \frac{\zeta_\alpha^{-2}}{\left(\zeta_\alpha^{-1} - \bar{\hat{\zeta}}_k\right)^2}\frac{\mathrm{d}\zeta_\alpha}{\mathrm{d}z_\alpha}\frac{\partial z_\alpha}{\partial s}\frac{\mathrm{d}\bar{\hat{\zeta}}_k}{\mathrm{d}\bar{\hat{z}}_k}\frac{\partial \bar{\hat{z}}_k}{\partial \hat{x}_i} \gg \mathbf{B}^{-1}\bar{\mathbf{B}}\mathbf{I}_k\bar{\mathbf{A}}^{\mathrm{T}}$$

$$\frac{\partial \hat{z}_\alpha}{\partial \hat{x}_i} = \begin{cases} 1, & i = 1 \\ p_\alpha & i = 2 \end{cases}, \qquad \frac{\partial \bar{\hat{z}}_k}{\partial \hat{x}_i} = \begin{cases} 1, & i = 1 \\ \bar{p}_k & i = 2 \end{cases},$$

$$\frac{\mathrm{d}\hat{\zeta}_\alpha}{\mathrm{d}\hat{z}_\alpha} = \frac{2}{a}\left\{(1 - ip_\alpha c) - (1 + ip_\alpha c)\hat{\zeta}_\alpha^{-2} + \varepsilon\kappa(1 + ip_\alpha)\hat{\zeta}_\alpha^{\kappa-1} - \varepsilon\kappa(1 - ip_\alpha)\hat{\zeta}_\alpha^{-(\kappa+1)}\right\}^{-1}$$

$$\frac{\mathrm{d}\bar{\hat{\zeta}}_k}{\mathrm{d}\bar{\hat{z}}_k} = \frac{2}{a}\left\{\left(1 + i\bar{p}_k c\right) - \left(1 - i\bar{p}_k c\right)\bar{\hat{\zeta}}_k^{-2} + \varepsilon\kappa\left(1 - i\bar{p}_k\right)\bar{\hat{\zeta}}_k^{\kappa-1} - \varepsilon\kappa\left(1 + i\bar{p}_k\right)\bar{\hat{\zeta}}_k^{-(\kappa+1)}\right\}^{-1}. \tag{16c}$$

After obtaining ϵ_{ij} through Eq. (15), the stresses of interior point $\hat{\mathbf{x}}$ can be evaluated by the stress–strain law $\sigma_{ij} = C_{ijks}\epsilon_{ks}$. If we define

$$\boldsymbol{\sigma}_1 = \begin{Bmatrix} \sigma_{11} \\ \sigma_{12} \\ \sigma_{13} \end{Bmatrix}, \qquad \boldsymbol{\sigma}_2 = \begin{Bmatrix} \sigma_{21} \\ \sigma_{22} \\ \sigma_{23} \end{Bmatrix} \tag{17}$$

it can be proved that (Hwu, 1999)

$$\boldsymbol{\sigma}_1(\hat{\mathbf{x}}) = \mathbf{Q}\mathbf{u}_{,1}(\hat{\mathbf{x}}) + \mathbf{R}\mathbf{u}_{,2}(\hat{\mathbf{x}}),\ \boldsymbol{\sigma}_2(\hat{\mathbf{x}}) = \mathbf{R}^{\mathrm{T}}\mathbf{u}_{,1}(\hat{\mathbf{x}}) + \mathbf{T}\mathbf{u}_{,2}(\hat{\mathbf{x}}), \tag{18}$$

where $\mathbf{Q}$, $\mathbf{R}$, $\mathbf{T}$ have been defined in Eq. (3c), and $\mathbf{u}_{,1}$ and $\mathbf{u}_{,2}$ are given in Eq. (15).

5. SCF of holes

The high stress concentration found at the edge of a hole is of great practical importance. To denote the highest stress caused by the hole, the stress concentration factor (SCF) is usually used and defined to be the maximum stress at the hole boundary divided by the remote uniform stress. Since the hole is assumed to be traction-free, the only stress component around the hole is the hoop stress σ_{nn}. To find the maximum hoop stress, we first employ the formula given in Eq. (5a). By using chain rule, the definition of Eq. (17) and the relationship given in Eq. (2c) we obtain

$$\sigma_{nn} = -\mathbf{n}^{\mathrm{T}}(\theta)\boldsymbol{\phi}_{,m} = -\mathbf{n}^{T}(\theta)\left[\frac{\partial \boldsymbol{\phi}}{\partial x_1}\frac{\partial x_1}{\partial m} + \frac{\partial \boldsymbol{\phi}}{\partial x_2}\frac{\partial x_2}{\partial m}\right] = \mathbf{n}^{\mathrm{T}}(\theta)(\cos\theta\boldsymbol{\sigma}_1 + \sin\theta\boldsymbol{\sigma}_2). \tag{19}$$

Substituting Eq. (18) into Eq. (19) and setting $\hat{\mathbf{x}}$ on the value of $\hat{\zeta}_\alpha = e^{i\varphi}$, the hoop stress can bc expressed in terms of the displacements along the hole boundary as

$$\sigma_{nn} = \mathbf{n}^{\mathrm{T}}(\theta)\big(\cos\theta\mathbf{Q} + \sin\theta\mathbf{R}^{\mathrm{T}}\big)\mathbf{u}_{,1}(e^{i\varphi}) + \mathbf{n}^{\mathrm{T}}(\theta)(\cos\theta\mathbf{R} + \sin\theta\mathbf{T})\mathbf{u}_{,2}(e^{i\varphi}) \tag{20}$$

where, θ and φ are related by (Hwu, 1992)

$$\rho\cos\theta = a(\sin\varphi + k\varepsilon\sin k\varphi), \qquad \rho\sin\theta = -a(c\cos\varphi + k\varepsilon\sin k\varphi), \tag{21}$$

in which

$$\rho^2 = a^2\big\{k^2\varepsilon^2 + \sin^2\varphi + c^2\cos^2\varphi + 2k\varepsilon\sin\varphi\sin k\varphi - 2ck\varepsilon\cos\varphi\cos k\varphi\big\}$$

For an elliptical hole, a simple relation can be obtained by letting $\varepsilon = 0$. Substituting Eq. (15) into Eq. (20), we may further obtain an expression for the hoop stress written in terms of the displacements $\mathbf{u}_n$, and tractions $\mathbf{t}_n$ of remote boundary nodes. The result is

$$\sigma_{nn} = \sum_{n=1}^{N}\Big\{\big[\mathbf{\Omega}_1\mathbf{G}_{n,\,1} + \mathbf{\Omega}_2\mathbf{G}_{n,\,2}\big]\mathbf{t}_n - \Big[\mathbf{\Omega}_1\hat{\mathbf{Y}}_{n,\,1} + \mathbf{\Omega}_2\hat{\mathbf{Y}}_{n,\,2}\Big]\mathbf{u}_n\Big\} \tag{22}$$

$$\mathbf{\Omega}_1 = \mathbf{n}^{\mathrm{T}}(\theta)\big(\cos\theta\mathbf{Q} + \sin\theta\mathbf{R}^{\mathrm{T}}\big), \qquad \mathbf{\Omega}_2 = \mathbf{n}^{\mathrm{T}}(\theta)(\cos\theta\mathbf{R} + \sin\theta\mathbf{T}).$$

Due to the anisotropic characteristic of materials, uncertainty of the geometry profile, and the complexity of Eq. (22), it seems difficult to get the analytical solution of maximum hoop stress. To find the maximum stress concentration of the hole, a numerical technique like the nonlinear optimization may be employed.

6. SIF of cracks

For the crack problem, it is always interesting to know the stress intensity factors which are defined as (Broek, 1974)

$$\mathbf{K} = \begin{Bmatrix} K_{II} \\ K_I \\ K_{III} \end{Bmatrix} = \lim_{r\to 0}\sqrt{2\pi r}\,\mathbf{\sigma}_2 \tag{23}$$

where r is the distance ahead of the crack tip and $\mathbf{\sigma}_2$ can be obtained from Eqs. (15) and $(18)_2$. In Eq. (15), $\mathbf{G}_{n,\,i}$ and $\hat{\mathbf{Y}}_{n,\,i}$ are obtained by differentiating Eq. (10b) with respect to $\hat{x}_i$ and adding together the values contributed by the neighbor elements. The analytical expressions for the differentiation of $\hat{\mathbf{U}}$ and $\hat{\mathbf{T}}$ have been provided in Eq. (16). By substituting the conditions of $\hat{x}_1 \to a$, $\hat{x}_2 = 0$ and $\varepsilon = 0$, $c = 0$ into Eq. (23), we may derive a closed-form solution for the stress intensity factors as (Hwu, 1999)

$$\mathbf{K} = \sum_{n=1}^{N}\big\{\big[\mathbf{R}^{\mathrm{T}}\mathbf{G}^*_{n1} + \mathbf{T}\mathbf{G}^*_{n2}\big]\mathbf{t}_n - \big[\mathbf{R}^{\mathrm{T}}\mathbf{Y}^*_{n1} + \mathbf{T}\mathbf{Y}^*_{n2}\big]\mathbf{u}_n\big\} \tag{24a}$$

$$\mathbf{G}^*_{ni} = \lim_{\substack{\hat{x}_1 \to a \\ \hat{x}_2 = 0}} \sqrt{2\pi(\hat{x}_1 - a)}\mathbf{G}_{n,\,i}(\hat{\mathbf{x}})$$

$$= \int_{-1}^{1} \mathbf{U}^*_i(\xi)(\varpi_2 \ell_{m-1} + \varpi_1 \ell_m)\,\mathrm{d}\xi, \quad i = 1, 2 \tag{24b}$$

$$\mathbf{Y}^*_{ni} = \lim_{\substack{\hat{x}_1 \to a \\ \hat{x}_2 = 0}} \sqrt{2\pi(\hat{x}_1 - a)}\hat{\mathbf{Y}}_{n,\,i}(\hat{\mathbf{x}})$$

$$= \int_{-1}^{1} \mathbf{T}^*_i(\xi)(\varpi_2 \ell_{m-1} + \varpi_1 \ell_m)\,\mathrm{d}\xi, \quad i = 1, 2 \tag{24c}$$

$$\mathbf{U}^*_1 = \frac{1}{2\sqrt{\pi a}}\mathrm{Im}\left\{\mathbf{A} \ll \frac{1}{1-\zeta_\alpha} \gg \mathbf{A}^{\mathrm{T}} - \mathbf{A} \ll \frac{\zeta_\alpha}{1-\zeta_\alpha} \gg \mathbf{B}^{-1}\bar{\mathbf{B}}\bar{\mathbf{A}}^{\mathrm{T}}\right\},$$

$$\mathbf{U}^*_2 = \frac{1}{2\sqrt{\pi a}}\mathrm{Im}\left\{\mathbf{A} \ll \frac{p_\alpha}{1-\zeta_\alpha} \gg \mathbf{A}^{\mathrm{T}} - \sum_{k=1}^{3}\mathbf{A} \ll \frac{\bar{p}_k\zeta_\alpha}{1-\zeta_\alpha} \gg \mathbf{B}^{-1}\bar{\mathbf{B}}\mathbf{I}_k\bar{\mathbf{A}}^{\mathrm{T}}\right\}$$

$$\mathbf{T}^*_1 = \frac{1}{a\sqrt{\pi a}}\mathrm{Im}\left\{\mathbf{B} \ll \frac{\zeta_\alpha^2(s_1 + p_\alpha s_2)}{\left(\zeta_\alpha^2 - 1\right)(1-\zeta_\alpha)^2} \gg \left(\mathbf{A}^{\mathrm{T}} - \mathbf{B}^{-1}\bar{\mathbf{B}}\bar{\mathbf{A}}^{\mathrm{T}}\right)\right\},$$

$$\mathbf{T}^*_2 = \frac{1}{a\sqrt{\pi a}}\mathrm{Im}\left\{\mathbf{B} \ll \frac{p_\alpha\zeta_\alpha^2(s_1 + p_\alpha s_2)}{\left(\zeta_\alpha^2 - 1\right)(1-\zeta_\alpha)^2} \gg \mathbf{A}^{\mathrm{T}} - \sum_{k=1}^{3}\mathbf{B} \ll \frac{\bar{p}_\alpha\zeta_\alpha^2(s_1 + p_\alpha s_2)}{\left(\zeta_\alpha^2 - 1\right)(1-\zeta_\alpha)^2} \gg \mathbf{B}^{-1}\bar{\mathbf{B}}\mathbf{I}_k\bar{\mathbf{A}}^{\mathrm{T}}\right\} \tag{24d}$$

To evaluate the integrals $\mathbf{G}^*_{ni}$ and $\mathbf{Y}^*_{ni}$ from Eqs. (24b) and (24c) we should first express $\mathbf{U}^*_i$ and $\mathbf{T}^*_i$ of Eq. (24d) in terms of ξ. The connection between the integration variable ξ and the function variables ζ_α can be found by using the ξ–$\boldsymbol{x}$ relation given in Eq. (10b), the $\boldsymbol{x}$–z_α relation given in Eq. (2b), and z_α–ζ_α relation given in Eq. (7).

Note that Eq. (24) provides a direct method for evaluating the stress intensity factor if the remote displacements $\mathbf{u}_n$ and tractions $\mathbf{t}_n$ are known on some closed contour containing the crack. The data on the remote closed contour may also be supplied by any other method like the finite element method or the experimental measurement. This is very different from the conventional computation of the stress intensity factors since they are usually obtained from the data near the crack tip. Even by the well-known path independent J-integral (Rice, 1968), we use a path starting and ending at the crack surfaces, while by Eq. (24), all the data used to calculate $\mathbf{K}$ are from the remote boundary. Using the conventional finite element to find a convergent solution for the stress intensity factors usually requires fine meshes near the crack tips. This is not only time consuming but also inaccurate. All these defects have been overcome by the present BEM since the crack need not be meshed and the stress intensity factors can be obtained using only the remote boundary displacements and tractions.

7. Numerical examples

To show that the proposed formulae obtained in Eq. (22) for SCF of holes, and Eq. (24) for SIF of cracks are accurate, efficient and versatile, several examples are illustrated in this section. All the examples shown in this section consider a rectangular plate containing a hole (or crack). A uniform tension $\sigma_0 = 1$ MPa in the x_2-direction is applied on the plate boundary and the plate size is $W = H = 0.3$ m. The plate is composed of the orthotropic material whose mechanical properties are $E_1 = 114.8$ GPa, $E_2 = E_3 = 11.72$ GPa, $G_{12} = G_{13} = G_{23} = 9.65$ GPa, $\nu_{12} = \nu_{13} = \nu_{23} = 0.21$. (x_c, y_c) denotes the position of the center of the hole(or crack). θ_c denotes the hole(or crack) orientation directed counterclockwise from the x_1-axis. (see Fig. 2).

Example 1: SCF of holes

Table 1 shows the results of SCF at position $\varphi = 0^\circ$ of various centered-holes. Two different methods are used to calculate SCF. One is by Eq. (22), and the other is by direct calculation of the hoop stress. To show that the values of $\mathbf{u}_n$, and $\mathbf{t}_n$ of the remote boundaries used in Eq. (22) can also be supplied by other sources, the results calculated by the commercial finite element code IDEAS are also compared. From this table it can easily be seen that all the results are similar no matter what kind of method is used. The main difference is that the CPU time for computing SCF by the present BEM method is much faster than that by IDEAS. Moreover, the use of Eq. (22) may also help IDEAS to obtain SCF more quickly (about four times faster).

To know the hoop stress distribution along the hole boundary, the case of the triangular hole was taken up as an illustration and its results are plotted in Fig. 3. From this figure, we see that the maximum hoop stress does not necessarily occur at the position,$\varphi = 0^\circ$. The maximum hoop stress is a compressive stress occurring at $\varphi = 100.8^\circ$ and $\varphi = 259.2^\circ$, and its value is $6.297\sigma_0$. While the maximum tensile hoop stress occurs at $\varphi = 0^\circ$ whose value is $4.654\sigma_0$.

The convergence of SCF with respect to the element number is shown in Fig. 4 for the present BEM and IDEAS. From this figure, we can get the complete comparison between these two methods. Only 16 elements, that BEM needed, can obtain the convergence value of SCF, but

Table 1
SCF at the position $\varphi = 0^\circ$ of various centered-holes ($a/W = 0.1, x_c/W = 0.5, y_c/W = 0.5, \theta_c = 0^\circ$)

		BEM[a]		FEM[b]			
		SCF	CPU[c]	SCF	CPU[c]	Nodes	Elements
Circle ($c = l$, $\varepsilon = 0$)	Eq. (22)	2.531	1.71 s	2.527	14.28 s	1016	318
	Hoop solution	2.530	1.69 s	2.518	49.44 s	3435	1084
Ellipse ($c = 0.6$, $\varepsilon = 0$)	Eq. (22)	3.403	1.71 s	3.371	14.29 s	1016	318
	Hoop solution	3.403	1.69 s	3.359	45.34 s	3148	1000
Triangle ($c = 1$, $\varepsilon = 0.15$, $\kappa = 2$)	Eq. (22)	3.758	6.02 s	3.713	22.81 s	1114	334
	Hoop solution	3.757	5.98 s	3.687	72.38 s	4824	1456
Square ($c = 1$, $\varepsilon = 0.15$, $\kappa = 3$)	Eq. (22)	4.201	7.79 s	4.128	21.58 s	1108	332
	Hoop solution	4.200	7.70 s	4.103	55.93 s	3880	1232
Pentagon ($c = 1$, $\varepsilon = 0.15$, $\kappa = 4$)	Eq. (22)	5.564	11.24 s	5.479	30.14 s	1196	344
	Hoop solution	5.563	11.08 s	5.413	164.55 s	7907	2527

[a] Present BEM solution with 16 elements and 20 nodes.
[b] Based upon the data provided by IDEAS.
[c] All calculations are executed in HP9000-735 workstation with 120MB RAM.

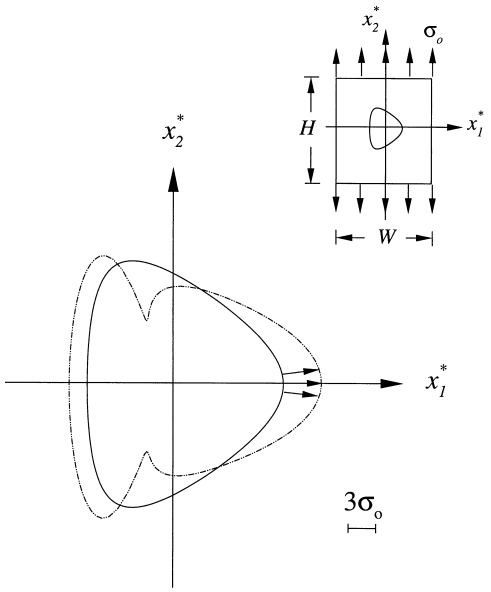

Fig. 3. Hoop stress around the triangular hole. ($a/W = 0.2$, $c = 1$, $k = 2$, $\varepsilon = 0.15$, $(x_c/W, y_c/W) = (0.5, 0.5)$)

IDEAS needed 3084 elements to converge SCF. Although we spent much time preparing the Green's function of BEM, the higher computational speed and element saving make the present BEM attractive.

Table 2 lists the SCF of triangular holes of different sizes and locations. For the centered-holes of different sizes, the maximum tensile stress always occurs at $\varphi = 0^\circ$ and the maximum compressive stress

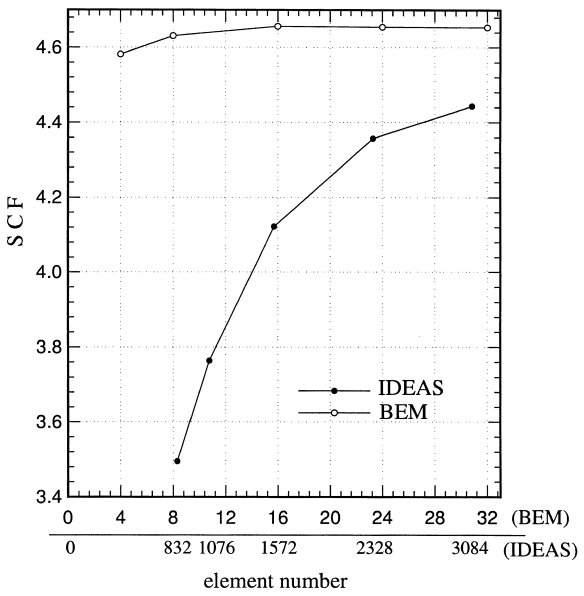

Fig. 4. Convergence of SCF with respect to the element number.

Table 2
SCF of various triangular holes[a] ($c = 1$, $\kappa = 2$, $\varepsilon = 0.15$)

Centered holes of different sizes ($x_c/W = y_c/W = 0.5$)									
a/W		0.067	0.100	0.133	0.167	0.200	0.233	0.267	0.300
SCF^T	$\varphi = 0^\circ$	3.5863	3.7576	3.9976	4.2467	4.6544	5.1717	5.9545	7.1014
SCF^C	$\varphi = 100.8^\circ$, 259.2°	3.4819	4.1488	4.8040	5.2800	6.2971	7.5328	9.3204	11.5653

Holes of different locations ($a/W = 0.1$)										
x_c/W		0.3	0.4	0.5	0.6	0.7	0.7	0.7	0.7	0.7
y_c/W		0.7	0.7	0.7	0.7	0.7	0.6	0.5	0.4	0.3
SCF^T	$\varphi = 0^\circ$	3.7919	3.8440	3.8561	3.8948	4.0123	3.9827	3.9797	4.0566	4.0223
SCF^C	$\varphi = 100.8^\circ$	4.7485	4.4546	4.4335	4.4746	4.7190	4.5729	4.4905		
SCF^T	$\varphi = 259.2^\circ$								4.5682	4.7772

[a] SCF^T: SCF for maximum tensile stress; SCF^C: SCF for maximum compressive stress.

always occurs at,$\varphi = 100.8^\circ$ and $\varphi = 259.2^\circ$. Moreover, the bigger the hole size, the larger the SCF. For holes of different locations, the maximum tensile stress still occurs at $\varphi = 0^\circ$ while the maximum compressive stress occurs at $\varphi = 100.8^\circ$ or $\varphi = 259.2^\circ$ depending on its location. Moreover, the SCF is higher when the hole is closer to the plate boundary, which is reasonable.

Table 3
Stress intensity factor K_I of the right tip of various cracks

$2a/W$	(x_c, y_c)	θ_c		BEM[a]		FEM[b]			
				K_I (MPa $\sqrt{m}$)	CPU[c] (s)	K_I (MPa $\sqrt{m}$)	CPU[c] (s)	Nodes	Elements
0.4	(0.5, 0.5)	0°	Eq. (24)	0.477	1.71	0.441	54.21	1604	442
			Near tip solution	0.475	1.69	0.432	221.32	14728	4802
0.2	(0.5, 0.5)	0°	Eq. (24)	0.314	1.71	0.305	54.21	1604	442
			Near tip solution	0.313	1.69	0.301	219.36	14726	4800
0.3	(0.7, 0.5)	0°	Eq. (24)	0.420	1.73	0.403	54.21	1604	442
			Near tip solution	0.418	1.70	0.392	223.40	14732	4800
0.3	(0.7, 0.7)	0°	Eq. (24)	0.424	1.73	0.411	54.21	1604	442
			Near tip solution	0.422	1.70	0.397	224.01	14736	4800
0.3	(0.5, 0.5)	15°	Eq. (24)	0.371	1.74	0.352	59.75	1684	484
			Near tip solution	0.370	1.71	0.340	288.73	15706	5126
0.3	(0.5, 0.5)	30°	Eq. (24)	0.304	1.73	0.271	59.75	1684	484
			Near tip solution	0.303	1.70	0.262	291.27	15844	5153
0.3	(0.5, 0.5)	45°	Eq. (24)	0.207	1.73	0.196	59.75	1684	484
			Near tip solution	0.207	1.70	0.181	297.54	16096	5204
0.3	(0.5, 0.5)	60°	Eq. (24)	0.106	1.73	0.094	59.75	1684	484
			Near tip solution	0.105	1.70	0.086	294.12	15964	5176
0.3	(0.5, 0.5)	75°	Eq. (24)	0.027	1.74	0.023	59.75	1684	484
			Near tip solution	0.026	1.71	0.021	295.38	16008	5184
0.3	(0.5, 0.5)	90°	Eq. (24)	0.003	1.73	0.001	59.75	1684	484
			Near tip solution	0.003	1.70	0.001	293.15	15922	5168

[a] Present BEM solution with 16 elements and 20 nodes.
[b] Based upon the data provided by IDEAS.
[c] All calculations are executed in HP9000-735 workstation with 120 MB RAM.

Example 2: SIF of cracks

The calculation of the stress intensity factors are usually done by using the near tip solutions. To see the accuracy and efficiency of the present method, Table 3 shows the SIFs of the right tip of various cracks calculated by Eq. (24) as well as those by the near tip solution both through the present BEM and IDEAS. Same as the hole problems, our results calculated indirectly by the boundary displacements and tractions are near to those obtained directly by the near tip solutions. The CPU time for computing SIF by the present BEM method is over 100 times faster than that by IDEAS. Moreover, the use of Eq. (24) may also help IDEAS to obtain SIF more quickly (about four times faster).

8. Conclusions

In this paper, two analytical formulae expressed in terms of the remote boundary tractions and displacements have been obtained. One is for the evaluation of the stress concentration factors of internal elliptical or polygon-like holes, the other is for the stress intensity factors of internal straight cracks. Both of them are valid for two-dimensional linear anisotropic elastic problems. Although the analytical solutions have a complex mathematical form, numerical implementation proves that they are really accurate, efficient and versatile. Moreover, the displacements and tractions of the remote boundaries can also be supplied by any other method like the finite element method or by experimental measurement.

Acknowledgements

The authors would like to thank the National Science Council for their support through grants NSC 85-2212-E006-059 and NSC 87-2212-E-006-090.

References

Anderson, T.L., 1991. Fracture Mechanics — Fundamentals and Applications. CRC Press, Boca Raton.

Broek, D., 1974. Elementary Engineering Fracture Mechanics. Noordhoff, Leyden.

Chen, F.H.K., Shield, R.T., 1977. Conservation laws in elasticity of the *J*-integral type. Z. Angw. Math. Phys 28, 1–22.

Hwu, C., 1990. Anisotropic plates with various openings under uniform loading or pure bending. ASME J. Applied Mechanics 57, 700–706.

Hwu, C., Yen, W.J., 1991. Green's functions of two-dimensional anisotropic plates containing an elliptic hole. Int. J. Solids and Structures 27 (13), 1705–1719.

Hwu, C., 1992. Polygonal holes in anisotropic media. Int. J. Solids and Structures 29, 2369–2384.

Hwu, C., Liao, C.Y., 1994. A special boundary element for the problems of multi-holes, cracks and inclusions. Computers and Structures 51 (1), 23–31.

Hwu, C., 1999. A new BEM for two-dimensional anisotropic elastic solids containing multiple holes, cracks and inclusions. In: Bush, M.B. (Ed.), Discontinuous Materials and Structures, Advances in Boundary Element Series. WIT Press/Computational Mechanics Publications, Southampton, UK (Chapter 2).

Lekhnitskii, S.G., 1968. Anisotropic Plates. Gordon and Breach/MIR, London/Moscow.

Murakami, Y., 1987. Stress Intensity Factors Handbook, vols. 1–2. Pergamon Press, Oxford.

Owen, D.R.J., Fawkes, A.J., 1983. Engineering Fracture Mechanics: Numerical Methods and Applications. Pineridge Press, Swansea, UK.

Rice, J.R., 1968. A path independent integral and the approximate analysis of strain concentration by notches and cracks. J. Applied Mechanics 35, 379–386.

Savin, G.N., 1961. Stress Concentration Around Holes. Pergamon Press, Oxford.

Sokolnikoff, I.S., 1956. Mathematical Theory of Elasticity. McGraw-Hill, New York.
Stroh, A.N., 1958. Dislocations and cracks in anisotropic elasticity. Philosophical Magazine 7, 625–646.
Ting, T.C.T., 1996. Anisotropic Elasticity — Theory and Applications. Oxford Science, New York.
Wang, Y.M., Tarn, J.Q., 1993. Green's functions for general plane problems of anisotropic bodies with a hole or a rigid inclusion. ASME J. Applied Mechanics 60, 583–588.
Wu, K.C., 1989. Representations of stress intensity factors by path-independent integrals. ASME J. Applied Mechanics 56, 780–785.
Yau, J.F., Wang, S.S., Corten, H.T., 1980. A mixed mode crack analysis of isotropic solids using conservation laws of elasticity. ASME J. Applied Mechanics 47, 335–341.